Generation of plasmaspheric undulations

N. Buzulukova,[1,2] M.-C. Fok,[1] T. E. Moore,[1] and D. M. Ober[3]

Received 28 March 2008; revised 15 May 2008; accepted 2 June 2008; published 11 July 2008.

[1] We have modeled the plasmaspheric plume region using the Comprehensive Ring Current model (CRCM) and the Dynamical Global Core Plasma model (DGCPM), for an event that exhibited substantial undulations or ripples as observed by the IMAGE EUV imager during 17 April 2002. We drove the simulated electric field using the Weimer cross polar cap potential. We specified the magnetic field to vary in response to solar wind conditions according to the T96 model. As a control, we performed a run with a fixed magnetic field and a run with a low ring current pressure. The results show that particle injections into the inner magnetosphere and ring current–ionosphere–plasmasphere interaction are an essential part of the undulation response. We also conclude that the undulations are stronger in the case of magnetic field variations because associated induction electric field causes more pronounced injections. **Citation:** Buzulukova, N., M.-C. Fok, T. E. Moore, and D. M. Ober (2008), Generation of plasmaspheric undulations, *Geophys. Res. Lett.*, *35*, L13105, doi:10.1029/2008GL034164.

1. Introduction

[2] Since its discovery almost forty years ago, the plasmasphere (hereafter PSP) has been intensively studied both theoretically and experimentally [see *Lemaire and Gringauz*, 1998, and references therein]. With launching of IMAGE satellite in 2000 a new era of PSP exploration began. EUV images of PSP provided by IMAGE have confirmed our basic knowledge about PSP dynamics and formation of global structures such as plasmaspheric body tail/plume [*Sandel et al.*, 2003]. A comprehensive description of different mechanisms of PSP and plasmaspheric tail formation is given by *Lemaire and Gringauz* [1998, chap. 5] and *Ganguli et al.* [2000]. IMAGE observations also show that the shape of the PSP has a number of new features: ''crenulations'', ''notches'', ''shoulders'', ''channels'' [*Sandel et al.*, 2003; *Spasojević et al.*, 2003] and transient ''undulations'' and ''ripples'' [*Goldstein et al.*, 2005]. Shoulder and channel formation seems to relate with periods of weak convection [*Goldstein et al.*, 2003; *Spasojević et al.*, 2003]. The origin of crenulations, notches and ripples is understood rather poorly. It is proposed that the formation of these structures is related with substorm development and with particle injections during substorm [*Goldstein et al.*, 2005; *Fok et al.*, 2005], but the details are still unclear.

[3] The goal of this work is to describe first results from detailed theoretical investigation of plasmaspheric ripples and undulations. In particular we consider modeling of 17 April 2002 event when IMAGE observed well-defined undulation/ripples of the PSP [*Goldstein et al.*, 2005]. We study the influence of dynamic magnetic B-field and convective E-field on plasmapause formation and propose a mechanism for undulation/ripples formation which is consistent with observational characteristics reported by *Goldstein et al.* [2005]. In what follows, we describe and model a specific event and draw conclusions regarding magnetosphere-ionosphere-PSP coupling during undulation/ripples events and the relations between ripples, particle injections and ring current undulations.

2. 17 April 2002 Event

[4] The geomagnetic storm on 17 April 2002 was a moderate one with commencement at ~11 UT and Dst minimum value of −98 nT at ~19 UT (for a detailed description of this storm and solar wind (SW) and interplanetary magnetic field (IMF) conditions see, e.g., *Liemohn et al.* [2004]). During this event IMAGE captured a number of clear plasmaspheric pictures, including well-defined ripples and undulations at 19–20:30 UT. *Goldstein et al.* [2005] provided a detailed description of this event. *Fok et al.* [2005] described a PSP-ring current-radiation belt model and reported a modeled PSP ripple for 17 April 2002 event. They pointed out the importance of ring current injection for ripple formation. However, no detailed analysis was made and the role of induction E-field was omitted. Also, several other works have described the results of PSP modeling during 17 April 2002, but none of them consider ripples/undulations [e.g., *Liemohn et al.*, 2004].

3. Description of the Models

[5] The Comprehensive Ring Current Model (CRCM) [*Fok et al.*, 2001] and Dynamical Global Core Plasma Model (DGCPM) [*Ober et al.*, 1997] were used to calculate ring current fluxes, electric fields, field-aligned currents and plasmaspheric density in the inner magnetosphere. CRCM is a kinetic model of the ring current (RC) particles, included H^+ and e^- (in our case). CRCM solves the bounce-averaged Boltzmann equation to obtain temporal evolution of four dimensional phase space density, specified by two ionospheric coordinates (Λ and MLT) and two adiabatic invariants μ and K. CRCM model also calculates Region II field-aligned currents and ionospheric electric field potential which are consistent with particle pressure distribution. The effect of inductive electric field is included implicitly via motion of flux tubes due to magnetic field reconfiguration. The basic equations and input/output parameters of CRCM are described elsewhere [*Fok et al.*, 2001, 2005], so we focus here only on specific details of the

[1]NASA Goddard Space Flight Center, Greenbelt, Maryland, USA.
[2]Space Research Institute (IKI), Moscow, Russia.
[3]Air Force Research Laboratory, Hanscom Air Force Base, Massachusetts, USA.

0094-8276/08/2008GL034164$05.00

model runs, namely for models of B-field and convection E-field, which must be specified externally.

[6] For the B-field we used T96 model [*Tsyganenko and Stern*, 1996] parametrized by SW density and velocity, IMF and Dst index. To separate an effect of convection E-field (E_{conv}) from effect of inductive E-field (E_{ind}) we performed two runs. In the first run, we averaged 1-min ACE SW and IMF data, shifted to bowshock, at 15 min intervals to produce input for T96 (dynamic B-field run, or DB-run for short). In the second run we used a steady inputs for T96 to obtain constant magnetic field (fixed B-field run, or FB-run for short). For both DB-run and FB-run we used linear dependencies from Nsw and Vsw to calculate plasma sheet density and temperature at the outer boundary [*Fok et al.*, 2005]. To isolate and identify the effect of RC pressure, we performed a run with dynamic B-field and a low RC pressure (DB-L-run in short). The value of boundary plasma density for this run was diminished by the factor of 5 in comparison with FB and DB-runs. For E_{conv} potential at the polar boundary of CRCM ($\Lambda = 68.3°$) we used the Weimer 2000 model [*Weimer*, 2001] parametrized by SW density, velocity and IMF. We also calculated cross polar cap potential (CPCP) as a potential drop along polar boundary. For all runs we averaged 1-min shifted ACE SW and IMF data to produce input for Weimer, T96 and plasma sheet models at 15 min intervals (except T96 input for FB-run).

[7] The DGCPM model calculates an equatorial plasmaspheric density versus time and describe $\mathbf{E} \times \mathbf{B}$ drift as well as refilling on the dayside and draining on the nightside (for details, see *Ober et al.* [1997] and *Fok et al.* [2005]). In our calculations we used the electric field as given by Weimer and magnetic field from T96, both the same as for CRCM, as inputs for DGCPM.

4. A Model Definition of Plasmapause and Ripples/Undulations

[8] From a ''classical'' definition, the plasmapause (hereafter PP) is a steep density gradient of cold H^+ [*Lemaire and Gringauz*, 1998]. Thus the PP could be considered as the H^+ edge of plasmasphere. In IMAGE data PP is also assumed to be the edge, but of He^+ emissions [*Sandel et al.*, 2003]. A relation between these two definitions has been proposed since [*Meier and Weller*, 1974]. Calculation of H^+/He^+ ratio and He^+ emissions is beyond the scope of this report, so we define PP as the edge where the value of plasma concentration obtained from CRCM/DGCPM equals 10 cm^{-3}. This value is close to IMAGE/EUV threshold 30–50 cm^{-3} which is obtained from EUV and in situ data comparison [*Sandel et al.*, 2003].

[9] A plasmaspheric undulation can be defined as a westward traveling wavy structure or a ripple along a PP [*Goldstein et al.*, 2005]. To extract ripples from CRCM/DGCPM results we plot modeled PP radius as a function of MLT for each time step for period 10–21 UT of April 17 2002. This is essentially the same approach as for IMAGE-derived PP location that is given by *Goldstein et al.* [2005, Figure 2], but for modeled PP. There is a region in which three different PP edges can be identified in the same MLT sector. This is the region of a plasmaspheric plume/tail. We identify the PP with the largest radius, because the ripples or undulations travel along the outermost plasmaspheric boundary.

5. Model Predictions

[10] Figure 1 shows the position of PP as a function UT (X axis) and MLT (Y axis). A vertical cut at some UT gives the PP position at 11–21 MLT. Darker color denotes the larger radius. Consider first the results for FB-run (Figure 1a). CPCP for this period (Figure 1b) exhibits a number of well-defined peaks and wells. The PP response reveals a complex behavior and is defined by ''outer'' SW imposed E-field, ''inner'' RC imposed E-field and the prehistory of PP position. We concentrate here on several oblique structures which appear on the eastern boundary of a plume in the evening sector. They exhibit wave-like variations in PP radius that travel along PP in westward direction. We identify these structures as a plasmaspheric ripples/undulations. The structure at 19–20 UT (ripple 1) corresponds well to observation of undulation/ripple by IMAGE. Figure 1c shows PP location for dynamic magnetic field run (DB-run). In this case, the PP is located at smaller radii, on average. Also, for the DB-run, the picture is significantly more structured. Oblique structures become more visible and a number of new ones appears. Figure 1d shows PP location for DB-L-run with low value of RC pressure. By that time, all oblique structures have disappeared. The main difference between DB-run and DB-L-run is the absence of RC electric field imposed from interaction with the ionosphere.

[11] Figure 2 shows a snapshot of plasmasphere-RC dynamics during ripples formation; top, middle and bottom strings present E_{conv} (corotation excluded) overlapped with field-aligned currents, E_{conv} (corotation included) overlapped with plasmasphere density, and RC pressure for 16–27 keV H^+. The first two columns show the ripple 1 onset from Figure 1a. At 18:46 UT, The RC shows a bulge structure near midnight, from newly injected particles during strong convection at 18–18:40 UT. The second small bulge arises in the evening sector and is formed by previously injected particles. As the CPCP decreases at 18:56 UT, bulges in RC begin to move westward due to gradient/curvature drift in weak E-field, that is similar to proton drift echo formation. Characteristic structures in Birkeland currents move in westward direction together with RC structures, producing changes in E-field pattern and PP undulation.

[12] An induction E-field causes deeper and stronger injections, so the ripples/undulations for DB-run are more pronounced. The 2nd and 3nd columns on Figure 2 show situation for UT 12:31 both for FB-run and DB-run. RC for DB-run reveals a newly injected population near midnight. This structure seems to arise from a combined effect of strong convection and E_{ind} motion during 12:00–12:20 UT, and is not so well developed for FB-run. RC at 12:41 UT for DB-run reveals somewhat wavy structure, originating from variable in time E_{ind}, which causes a number of injections and forms small bulges and concavities. When the CPCP decreased significantly at 12:50–13:20 UT, the bulges and concavities in RC began to move westward. For given energy, angular velocity of gradient/curvature drift is proportional to L (for dipole B-field), so drift of a small bulge

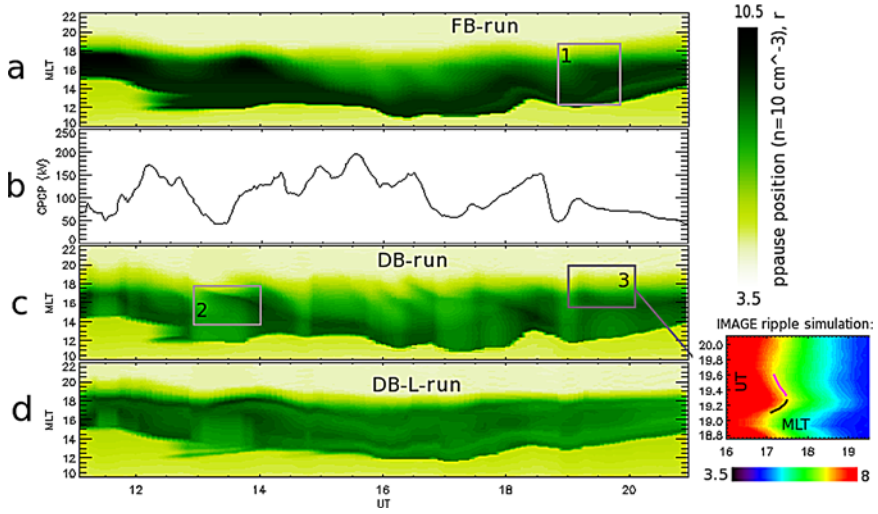

Figure 1. (a) Plasmapause position (in R_E, indicated by color scale) at the equatorial plane versus UT (X axis) and MLT (Y axis) for the case of a run with fixed B-field (FB-run). (b) Cross-polar cup potential at $\Lambda = 68.3°$ derived from Weimer model as a function from UT. (c) The same as Figure 1a but for the case of dynamic B-field run (DB-run). (d) The same as Figure 1c but for run with low ring current pressure (DB-L-run). Gray rectangles show three examples of ripples. An enlarged fragment shows the ripple 3 but in the format of *Goldstein et al.* [2005, Figure 2] for IMAGE–observed ripple. The PP definition is the same as for all runs. Black line denotes bulge PP motion and magenta line shows westward ripple motion.

causes steepening of edges, increasing the azimuthal pressure gradients and hence increasing the Birkeland currents via ''Vasyliunas loop''. It is also possible that there is development of secondary interchange-like instability [*Sazykin et al.*, 2002] because the PV^{γ} pattern also reveals complex structure near RC bulges and concavities (not shown here). A steep pressure gradients in RC causes strong field-aligned currents, changes in E-field pattern and PP

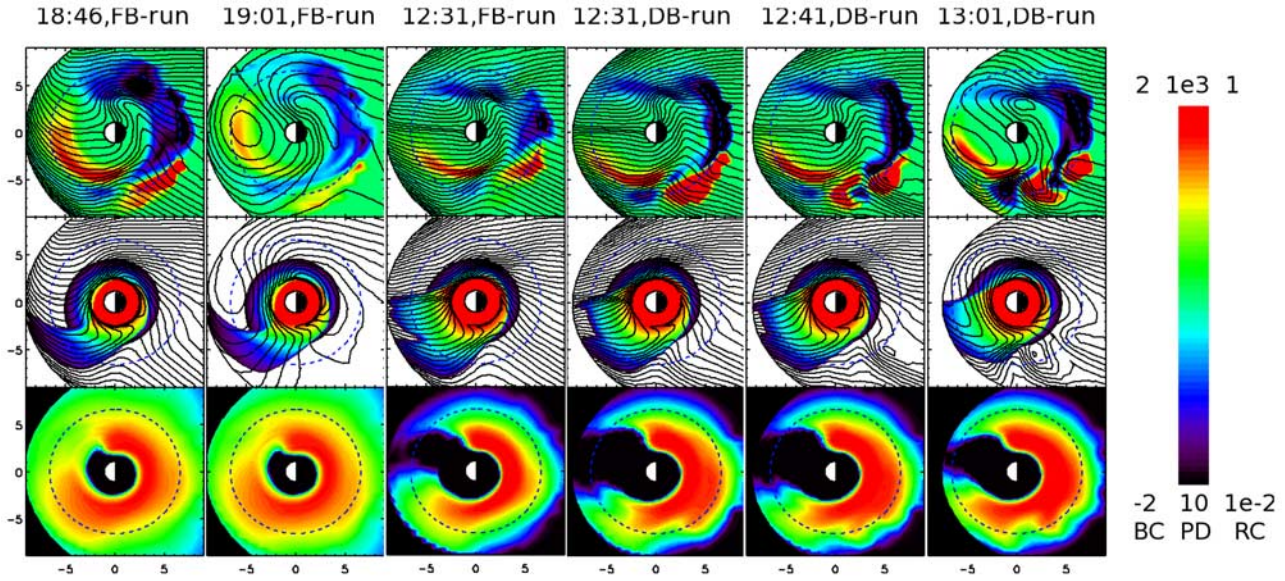

Figure 2. The formation of ripples 1 and 2 from Figure 1. String 1 shows snapshots of ionospheric Birkeland currents (BC, in color) overplotted with convection equipotentials; corotation is excluded. String 2 shows plasmaspheric density, (PD, in color, logarithmic scale) overplotted with convection equipotentials; corotation is included. String 3 shows ring current (RC) pressure for 16–27 keV H^+ (in color, logarithmic scale). All quantities are mapped on the equatorial plane. BC, PD and RC pressure are in $\mu A/m^2$, cm^{-3}, nPa, respectively. Equipotentials are 3 keV spacing. BC are positive down into the ionosphere. Sun is to the left. Dashed circles denote geostationary orbit. Two first columns show the onset of the ripple 1 formation for FB-run; the moving of RC inhomogeneities produces a ripple 1. The effect of E_{ind} on particle injection into RC is shown in the third column (FB-run) and the fourth column (DB-run); an enhanced injection for DB-run causes a ripple 2 formation (fifth and sixth columns).

undulations (ripple 2 in Figure 1c). When the potential increases significantly at 14:10 UT, all structures disappear.

6. Discussion

[13] Our results describe reasonably well the undulation observed by IMAGE at 19:00–20:30 UT. We obtained a well-defined undulation at 19–19:30 UT, although located slightly east of the IMAGE position. *Goldstein et al.* [2005] proposed the following sequence to explain observations: substorm injection; inflation of magnetic field due to injection in the evening; bulging of PP near injection; with SAPS/SAID development; giving ripple formation. An interval of positive SW Bz was not considered, though the onset of bulge formation just coincided with it.

[14] Owing to limitations of T96 model, we do not describe here substorm injection and E_{ind} consistently with phases of substorm development. Nevertheless, enhanced convection during 18:50–19 UT causes an injection and forms the inhomogeneities in RC. The bulge of the PP starts after overshielding and is presented in Figures 1a and 1c as the dark area at ~19 UT, just before ripples 1 and 3 begin to move in westward direction. Based on our results, we propose an alternate interpretation of the event: substorm injection; sharp CPCP drop in the end of injection; bulging of PP; ripple development through RC interactions; enhancement of convection and SAPS/SAID formation. In this interpretation, the positive SW Bz interval is an important part of undulation/ripple response because a lull in magnetospheric convection both amplifies an effect of RC imposed E-field and triggers westward motion of RC structures.

[15] It is possible that we underestimate the strength of convection and-or E_{ind}, because the bulge of RC injection is located at ~6–7 R_E at the equator (Figure 2, left column), while from HENA data it is located at ~3 R_E. This roughly coincides with the observed ripple location [*Goldstein et al.*, 2005]. As we explain the ripple by RC injection, we need to match the modeled PP with injection and put the PP further away from the Earth than the actual PP observed by IMAGE. This can perhaps explain why we need to choose the smaller threshold 10 cm^{-3} for PP instead 30–50 cm^{-3} obtained for EUV data.

[16] A wave-like structure in RC at 12:50–13:50 UT for the DB-run resembles the duskside diffuse auroral zone undulations that have been explained by Kelvin-Helmholtz instability and drift wave instability (for further details, see *Lewis et al.* [2005, and references therein]), or due to the interchange instability [*Sazykin et al.*, 2002]. However, the relations between different types of undulations and global dynamics of inner magnetosphere remain unclear, and will be the subject of future study.

7. Conclusions

[17] The simulation results presented here show that RC-plasmasphere-ionosphere interaction is an essential part of an undulation response. A strong convection and–or E_{ind} causes localized (in MLT) injection of plasma and formation of bulge-like structures in the RC. Azimuthal pressure gradients at the edges form field-aligned current, producing characteristic structures in E-field potential. After potential decrease, RC structures begin to move westward together with field-aligned current structures. This motion produces motion of E-field potential structures and ripples or undulations formation; E_{ind} amplifies this effect as it could produce more deep and pronounced injections. In some cases there may be development of secondary interchange-like instability in the RC plasma.

[18] **Acknowledgments.** This work was supported by an appointment to the NASA Postdoctoral Program at the Goddard Space Flight Center, administered by Oak Ridge Associated Universities through a contract with NASA. The ACE SW and IMF data were obtained from the GSFC/SPDF OMNIWeb interface at http://omniweb.gsfc.nasa.gov. The Dst, Kp and Ap indices were provided from the WDC for Geomagnetism, Kyoto.

References

Fok, M.-C., R. A. Wolf, R. W. Spiro, and T. E. Moore (2001), Comprehensive computational model of Earth's ring current, *J. Geophys. Res.*, *106*, 8417–8424, doi:10.1029/2000JA000235.

Fok, M.-C., Y. Ebihara, T. E. Moore, D. M. Ober, and K. A. Keller (2005), Geospace storm processes coupling the ring current, radiation belt and plasmasphere, in *Inner Magnetosphere Interactions: New Perspectives from Imaging*, *Geophys. Monogr. Ser.*, vol. 159, edited by J. Burch, M. Schulz, and H. Spence, pp. 207–220, AGU, Washington, D. C.

Ganguli, G., M. A. Reynolds, and M. W. Liemohn (2000), The plasmasphere and advances in plasmaspheric research, *J. Atmos. Sol. Terr. Phys.*, *62*, 1647–1657.

Goldstein, J., R. W. Spiro, B. R. Sandel, R. A. Wolf, S.-Y. Su, and P. H. Reiff (2003), Overshielding event of 28–29 July 2000, *Geophys. Res. Lett.*, *30*(8), 1421, doi:10.1029/2002GL016644.

Goldstein, J., J. L. Burch, B. R. Sandel, S. B. Mende, P. C. son Brandt, and M. R. Hairston (2005), Coupled response of the inner magnetosphere and ionosphere on 17 April 2002, *J. Geophys. Res.*, *110*, A03205, doi:10.1029/2004JA010712.

Lemaire, J. F., and K. I. Gringauz (1998), *The Earth's Plasmasphere*, Cambridge Univ. Press, New York.

Lewis, W. S., J. L. Burch, J. Goldstein, W. Horton, J. C. Perez, H. U. Frey, and P. C. Anderson (2005), Duskside auroral undulations observed by IMAGE and their possible association with large-scale structures on the inner edge of the electron plasma sheet, *Geophys. Res. Lett.*, *32*, L24103, doi:10.1029/2005GL024390.

Liemohn, M. W., A. J. Ridley, D. L. Gallagher, D. M. Ober, and J. U. Kozyra (2004), Dependence of plasmaspheric morphology on the electric field description during the recovery phase of the 17 April 2002 magnetic storm, *J. Geophys. Res.*, *109*, A03209, doi:10.1029/2003JA010304.

Meier, R. R., and C. S. Weller (1974), Extreme ultraviolet observations of the latitudinal variation of helium, *J. Geophys. Res.*, *79*, 1575–1578.

Ober, D. M., J. L. Horwitz, and D. L. Gallagher (1997), Formation of density troughs embedded in the outer plasmasphere by subauroral ion drift events, *J. Geophys. Res.*, *102*, 14,595–14,602, doi:10.1029/97JA01046.

Sandel, B. R., J. Goldstein, D. L. Gallagher, and M. Spasojević (2003), Extreme ultraviolet imager observations of the structure and dynamics of the plasmasphere, *Space Sci. Rev.*, *109*, 25–46, doi:10.1023/B:SPAC.0000007511.47727.5b.

Sazykin, S., R. A. Wolf, R. W. Spiro, T. I. Gombosi, D. L. De Zeeuw, and M. F. Thomsen (2002), Interchange instability in the inner magnetosphere associated with geosynchronous particle flux decreases, *Geophys. Res. Lett.*, *29*(10), 1448, doi:10.1029/2001GL014416.

Spasojević, M., J. Goldstein, D. L. Carpenter, U. S. Inan, B. R. Sandel, M. B. Moldwin, and B. W. Reinisch (2003), Global response of the plasmasphere to a geomagnetic disturbance, *J. Geophys. Res.*, *108*(A9), 1340, doi:10.1029/2003JA009987.

Tsyganenko, N. A., and D. P. Stern (1996), A new-generation global magnetosphere field model, based on spacecraft magnetometer data, *ISTP Newsl. 6*(1), p. 21, Int. Sol. Terr. Phys., NASA Goddard Space Flight Cent., Greenbelt, Md.

Weimer, D. R. (2001), An improved model of ionospheric electric potentials including substorm perturbations and application to the Geospace Environment Modeling November 24, 1996, event, *J. Geophys. Res.*, *106*, 407–416, doi:10.1029/2000JA000604.

N. Buzulukova, M.-C. Fok, and T. E. Moore, NASA Goddard Space Flight Center, Greenbelt, MD 20771, USA. (nbuzulukova@gmail.com)

D. M. Ober, Air Force Research Laboratory, Hanscom AFB, MA 01731, USA.